Journal of
Materials Chemistry B

Materials for biology and medicine

Accepted Manuscript

This article can be cited before page numbers have been issued, to do this please use: J. Ling, C. Pang, Y. Tan and L. Hong, *J. Mater. Chem. B*, 2025, DOI: 10.1039/D5TB01507C.

ROYAL SOCIETY OF CHEMISTRY

rsc.li/materials-b

View Article Online
DOI: 10.1039/D5TB01507C

Light-Activated Antimicrobial Polymers with Citronellol-Enhanced Bacterial Accumulation for On-Demand Disinfection

*Jiahao Ling[#], Chuming Pang[#], Yingxin Tan and Liangzhi Hong**

School of Materials Science and Engineering, Guangdong Provincial Key Laboratory of Luminescence from Molecular Aggregates, South China University of Technology, Guangzhou, 510640, China. E-mail: mslzhong@scut.edu.cn

[#] *Jiahao Ling and Chuming Pang contributed equally to this work*

Abstract: Antibacterial photodynamic therapy offers a promising approach to combating both susceptible and multidrug-resistant pathogens. However, conventional photosensitizers have limitations in terms of poor binding specificity and weak penetration for pathogens. In this study, we developed synergistic photobactericidal polymers that integrate hydrophilic toluidine blue O (TBO) with the lipophilic penetration enhancer citronellol (CT). The CT-containing monomer was copolymerized with glycidyl methacrylate, and then TBO was introduced *via* the epoxy group's ring-opening reaction. By combining the cationic charge and singlet oxygen ($^1O_2$) generation abilities of TBO with citronellol's membrane disrupting ability, the resulting copolymers have enhanced antimicrobial efficacy against Gram-positive, Gram-negative, and multidrug-resistant bacteria. CT not only enables the polymer to self-assemble and enhances the interaction between the polymer and bacteria, but also promotes the accumulation of TBO within cells by improving membrane permeability. $^1O_2$ generated in specific subcellular regions maximize photodynamic therapy's therapeutic potential. Furthermore, these copolymers can be used to develop light-activated antimicrobial polydimethylsiloxane that prevents bacterial adhesion and enables on-demand disinfection.

Keywords: photodynamic therapy, toluidine blue o, citronellol, synergistic antibacterial effect

View Article Online
DOI: 10.1039/D5TB01507C

1. Introduction

The global spread of COVID-19 underscored the persistent threat of microbial infections, particularly those caused by bacteria and viruses. [1-5] Antibiotics remain the cornerstone of the treatment of bacterial infections, however, the overuse and misuse of these drugs has resulted in the emergence of drug-resistant strains. [6-8] The mechanisms underlying bacterial drug resistance are complex and involve both genetic and biochemical pathways. Genetic mechanisms primarily include transduction, mutation, and transformation-replacement, whereas biochemical mechanisms encompass target modifications, reduced drug uptake, enhanced permeability barriers, impaired active membrane transport, and the activation of bacterial efflux systems. [9, 10] These challenges highlight the urgent need for development of novel and highly effective antibacterial systems that minimize the risk of developing drug resistance.

Antibacterial photodynamic therapy (aPDT) is an emerging antimicrobial treatment that utilizes light-activated photosensitizers to generate reactive oxygen species (ROS). [11-17] These ROS induce bacterial cell death by causing oxidative damage to proteins, nucleic acids, and lipids, as well as disrupting cellular metabolism. Notably, aPDT exhibits a lower likelihood of inducing bacterial drug resistance compared to conventional antibiotic treatments. [18-23] As singlet oxygen ($^1O_2$) diffuses only over short distances before quenching, effective aPDT requires a close spatial proximity between the photosensitizer and the target. [24] Toluidine blue O (TBO), a safe and effective cationic phenothiazine-type photosensitizer, has been widely employed in antibacterial applications, particularly for targeting oral pathogens. [25-29] Nevertheless, due to limited solubility in hydrophobic media and the strong hydrophilicity of TBO, its affinity for bacterial membrane lipids is reduced, leading to a reduction in its ability

View Article Online
DOI: 10.1039/D5TB01507C

to penetrate phospholipid bilayers, accumulate intracellularly, and maintain therapeutic concentrations in cells. [30-32] To overcome this limitation, TBO was incorporated into a gel system for acne treatment to prolong the TBO retention time. [30] Encapsulating TBO in appropriate nanocarriers could also increase cellular uptake. [33] In addition, TBO were conjugated with fatty acids to increase its hydrophobicity that would allow it to accumulate into biological membranes. [31] In recent studies, TBO combined with caffeic acid was found to improve the efficacy of aPDT and minimize toxicity. [32]

Citronellol (CT) is an acyclic biogenic monoterpenoid alcohol commonly found in the essential oils of aromatic plants. [34] It is a generally recognized as safe substance (GRAS) that may be used in food, cosmetics, and pharmaceuticals. [35] CT has achieved substantial commercial value in the flavor and fragrance industries due to its rose-like aroma. In addition to its herbicidal and insect repellent properties, CT has attracted increasing attention for its broad-spectrum antimicrobial properties based on multiple bactericidal mechanisms. [36-38] However, CT's antibacterial activity remains constrained by inherent physicochemical limitations, such as low water solubility and high volatility. [39] To address these limitations, recent studies have explored the incorporation of CT into polymeric chains. [40-42] For instance, we recently synthesized citronellol–poly(*N*,*N*-dimethyl ethyl methacrylate) (CD) polymers, which demonstrated rapid and potent bactericidal activity against Gram-positive, Gram-negative, and drug-resistant bacterial strains, with minimal resistance development observed after fifteen serial bacterial passages. [40] In addition, CD can impart durable antibacterial properties to cotton textiles. Yook and coworkers developed citronellol-derived methacrylate polymers, systematically investigating the effects of functional interconnecting groups on their antimicrobial properties. [41] CT-derived monomers have also been successfully used to fabricate

View Article Online
DOI: 10.1039/D5TB01507C

intrinsically antibacterial photopolymerizable thermoset resins for advanced 3D printing applications. [42]

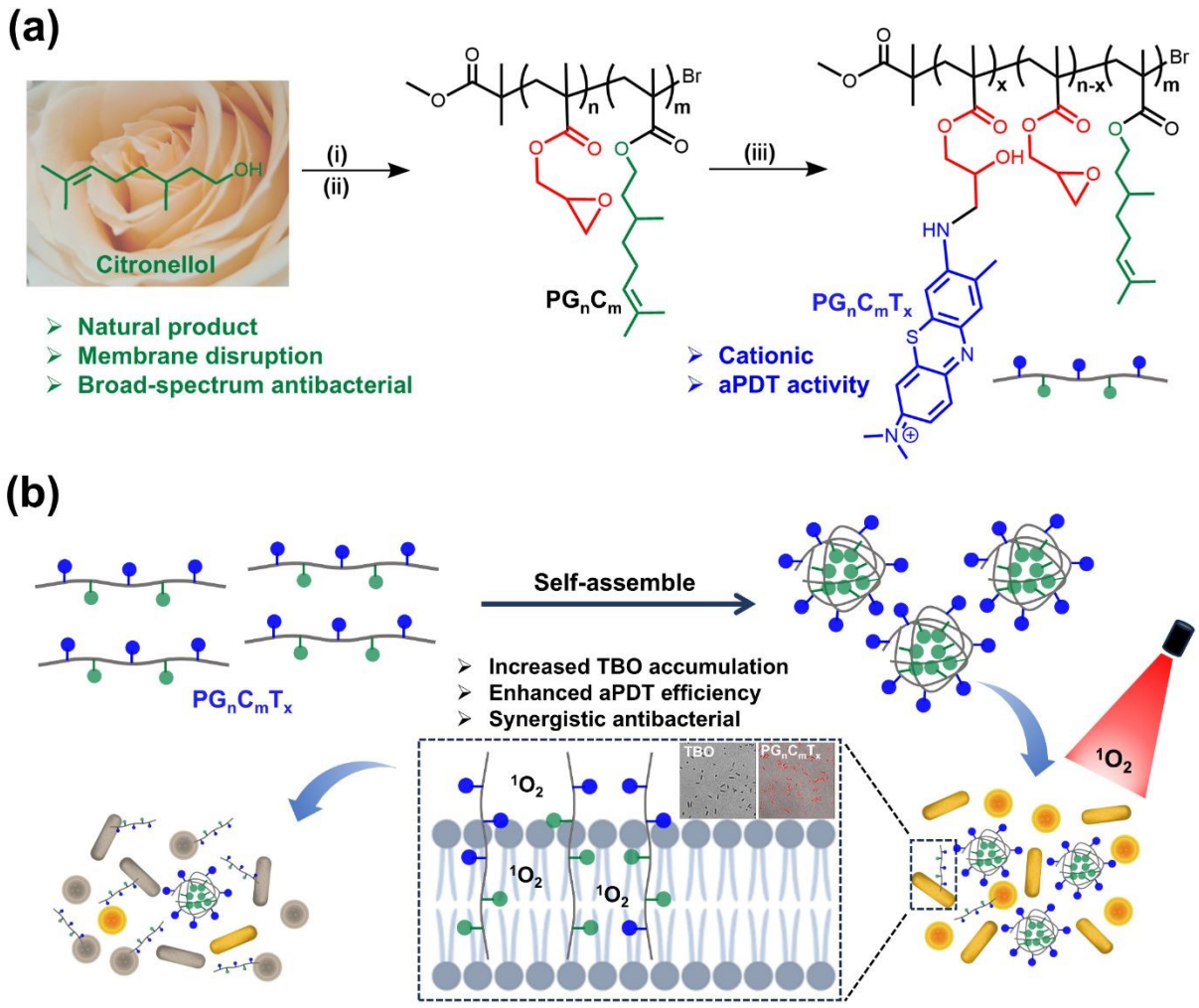

Figure 1. (a) Synthesis route of poly(glycidyl methacrylate-*co*-citronellol methacrylate-*co*-3-TBO-2-hydroxypropyl methacrylate) ($PG_nC_mT_x$). (i) Methacryloyl chloride, triethylamine, dichloromethane, 8 h; (ii) GMA, CuBr, 2,2′-bipyridine, THF, 50 °C, 12 h; (iii) TBO, DMSO, 25 °C, 2-8 h. (b) Self-assembly behavior of $PG_nC_mT_x$ and a Schematic illustration of synergistic aPDT process.

In this study, synergistic photobactericidal polymers containing hydrophilic TBO and

View Article Online
DOI: 10.1039/D5TB01507C

hydrophobic CT were developed in order to increase the effectiveness of aPDT against bacterial infections. The Poly(glycidyl methacrylate-*co*-citronellol methacrylate) copolymers bearing epoxy groups and citronellol groups in the side chains were prepared *via* living radical copolymerization of glycidyl methacrylate (GMA) and citronellol methacrylate (CMA) (Figure 1a). They were denoted as PG_nC_m, with n and m representing the degree of polymerization of GMA and CMA, respectively. The epoxy groups of PG_nC_m were then treated with TBO under mild conditions to produce ring-opening products poly(GMA-*co*-CMA-*co*-(2-hydroxy-3-TBO-propyl methacrylate)) ($PG_nC_mT_x$, where x denotes the number of ring-opening of GMA). The prepared $PG_nC_mT_x$ combines the cationic properties of TBO with its ability to generate $^1O_2$ and the lipophilicity of CT, resulting in significantly enhanced antibacterial activity (Figure 1b). Through a 'swell-encapsulation-shrink' method, we have also developed light-activated antimicrobial polydimethylsiloxane (LAPDMS) that prevents bacterial adhesion and enables on-demand disinfection.

2. Results and Discussion

2.1. Preparations and Characterizations of $PG_nC_mT_x$

The synthesis schematic of $PG_nC_mT_x$ is shown in Figure 1a. CMA was first synthesized by esterifying CT with methacryloyl chloride under alkaline conditions. PG_nC_m copolymers with controlled monomer ratios were prepared *via* atom transfer radical polymerization using methyl 2-bromoisobutyrate as the initiator, GMA and CMA as comonomers. The target $PG_nC_mT_x$ polymer was then formed by the reaction of the amine groups of TBO with the epoxy groups of PG_nC_m.

As shown in Figure 2a, the downfield shift of the signal corresponding to $H_{a'}$ in CMA occurs from 3.7 ppm to 4.2 ppm, while characteristic peaks of vinyl protons (H_c) were observed

View Article Online
DOI: 10.1039/D5TB01507C

at 5.6 ppm and 6.1 ppm, confirming that CMA had been successfully synthesized. A comparison of the ^{1}H NMR spectra of PG_9C_2 and $PG_9C_2T_7$ is shown in Figure 2b. The proton H_d at 3.63 ppm is specific to the initiator. Signals at 2.63, 2.83, 3.22, 3.78, and 4.3 ppm are attributed to H_g (2.63 and 2.83 ppm), H_f (3.22 ppm), and H_e (3.78 and 4.3 ppm) in GMA, and the signal at 5.1 ppm is attributed to $H_{b''}$ in CMA. For $PG_9C_2T_7$, signals in the range of 7.27–7.98 ppm, originating from the phenothiazine moiety of TBO (H_1, H_2, H_3 and H_4), enable the confirmation of its covalent conjugation *via* the epoxy ring-opening reaction. Based on the GPC analysis, all polymers showed narrow polydispersity. As summarized in Table 1, $PG_nC_mT_x$ polymers with different degrees of ring-opening were synthesized by precisely modulating the stoichiometry of the corresponding reactants. Additionally, $PG_9C_2T_7$ was found to self-assemble into a spherical nanoaggregate in aqueous solution (Figure 2c). The hydrodynamic diameter of $PG_9C_2T_7$ has been determined to be 174 nm by dynamic light scattering (Figure 2d). The critical micelle concentration (CMC) of $PG_9C_2T_7$ was determined to be approximately 62.5 $\mu g \cdot mL^{-1}$ using pyrene as a probe (Figure 2e).

View Article Online
DOI: 10.1039/D5TB01507C

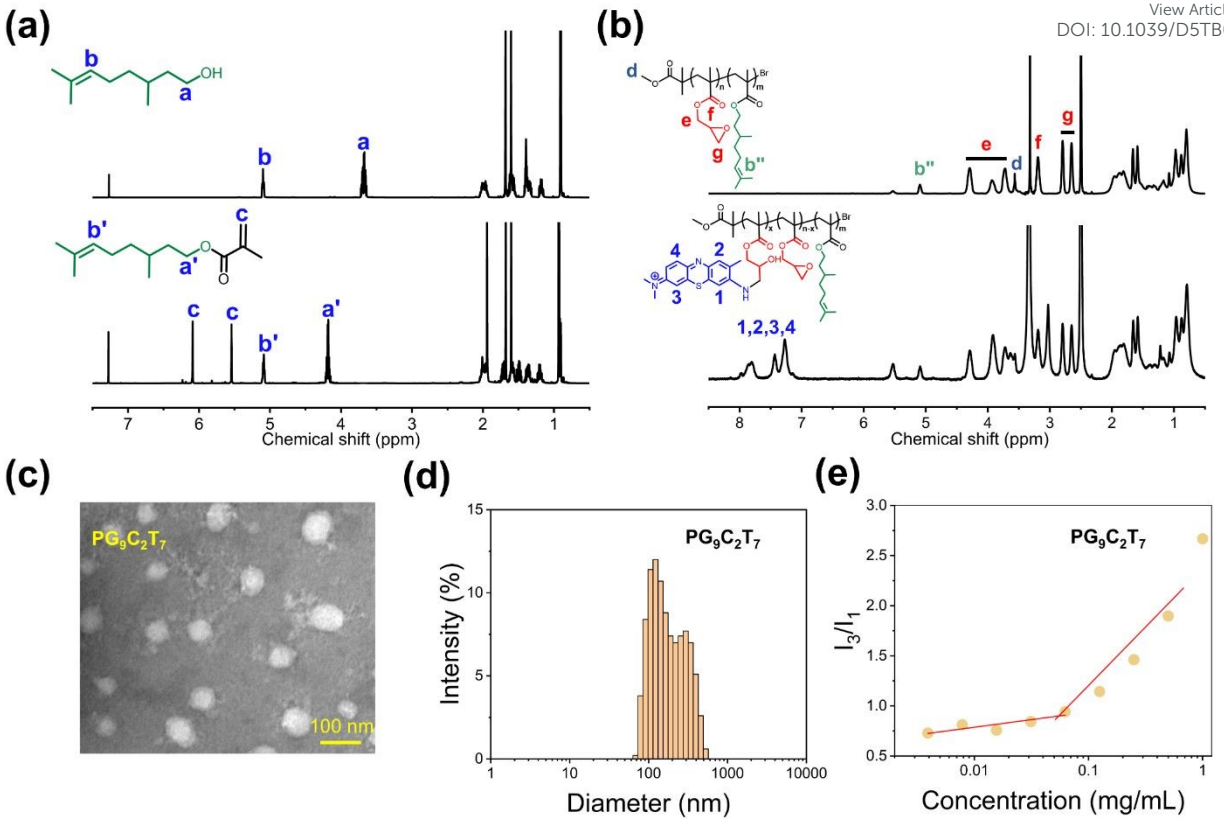

Figure 2. (a). ^{1}H NMR of CT and CMA. (b). ^{1}H NMR of PG_9C_2 and $PG_9C_2T_7$. (c) TEM image of $PG_9C_2T_7$ in water, negative staining with phosphotungstic acid. (d) Hydrodynamic diameter of $PG_9C_2T_7$ in water measured by dynamic light scattering. (e) CMC of $PG_9C_2T_7$ in water detected using a pyrene fluorescent probe.

Table 1. ^{1}H NMR and GPC Characteristics of PG_nC_m and $PG_nC_mT_x$.

Polymers	M_n[a]	PDI	Ring-Open degree[a]	Polymers	M_n[a]	PDI	Ring-Open degree[a]
PG_9C_2	1910	1.33	—	PG_6C_3	1709	1.31	—
$PG_9C_2T_9$	4662	—	100%	$PG_6C_3T_5$	3238	—	83%
$PG_9C_2T_7$	4050	—	77%	PG_6C_6	2384	1.33	—
$PG_9C_2T_4$	3133	—	44%	$PG_6C_6T_5$	3913	—	83%
$PG_9C_2T_2$	2522	—	22%	PG_9	1460	1.27	—
PG_9T_7	3601	—	77%				

View Article Online
DOI: 10.1039/D5TB01507C

[a] Determined by ^{1}H NMR, detailed spectra are shown in Figure s1-s11.

2.2. $^1O_2$ Formation Rate Constants

The generation of $^1O_2$ in $PG_nC_mT_x$ polymers was monitored by 1,3-diphenylisobenzofuran (DPBF), which is one of the most widely used $^1O_2$ probes because of its rapid reaction kinetics with $^1O_2$ and exceptional sensitivity to trace amounts of $^1O_2$. As a result of the irreversible reaction between DPBF and $^1O_2$, DPBF absorbance is pronouncedly reduced at 411 nm. [43, 44] The DPBF absorbance of samples treated with $PG_nC_mT_x$ declined rapidly (Figure 3a-3d), confirming the significant production of $^1O_2$ under light illumination. Various ring-opening degrees of polymer $PG_nC_mT_x$ exhibited significant DPBF attenuation profiles at varying irradiation times. Figure 3e shows the decay profiles of DPBF absorbance at 411 nm for CT, TBO, and $PG_nC_mT_x$. Pseudo-first-order model fitting was applied to the experimental data to better illustrate $^1O_2$ generation kinetics (Figure 3f). The rate constants for $^1O_2$ formation, calculated from the slopes of the first-order kinetic plots, were determined as 0.009 s^{-1}, 0.013 s^{-1}, 0.011 s^{-1}, 0.008 s^{-1} and 0.007 s^{-1} for TBO, $PG_9C_2T_9$, $PG_9C_2T_7$, $PG_9C_2T_4$ and $PG_9C_2T_2$, respectively. The comparable rates of $^1O_2$ generation between $PG_nC_mT_x$ polymers and TBO substantiate the polymers' effective photodynamic activity. In contrast, CT demonstrated negligible $^1O_2$ generation under light irradiation.

View Article Online
DOI: 10.1039/D5TB01507C

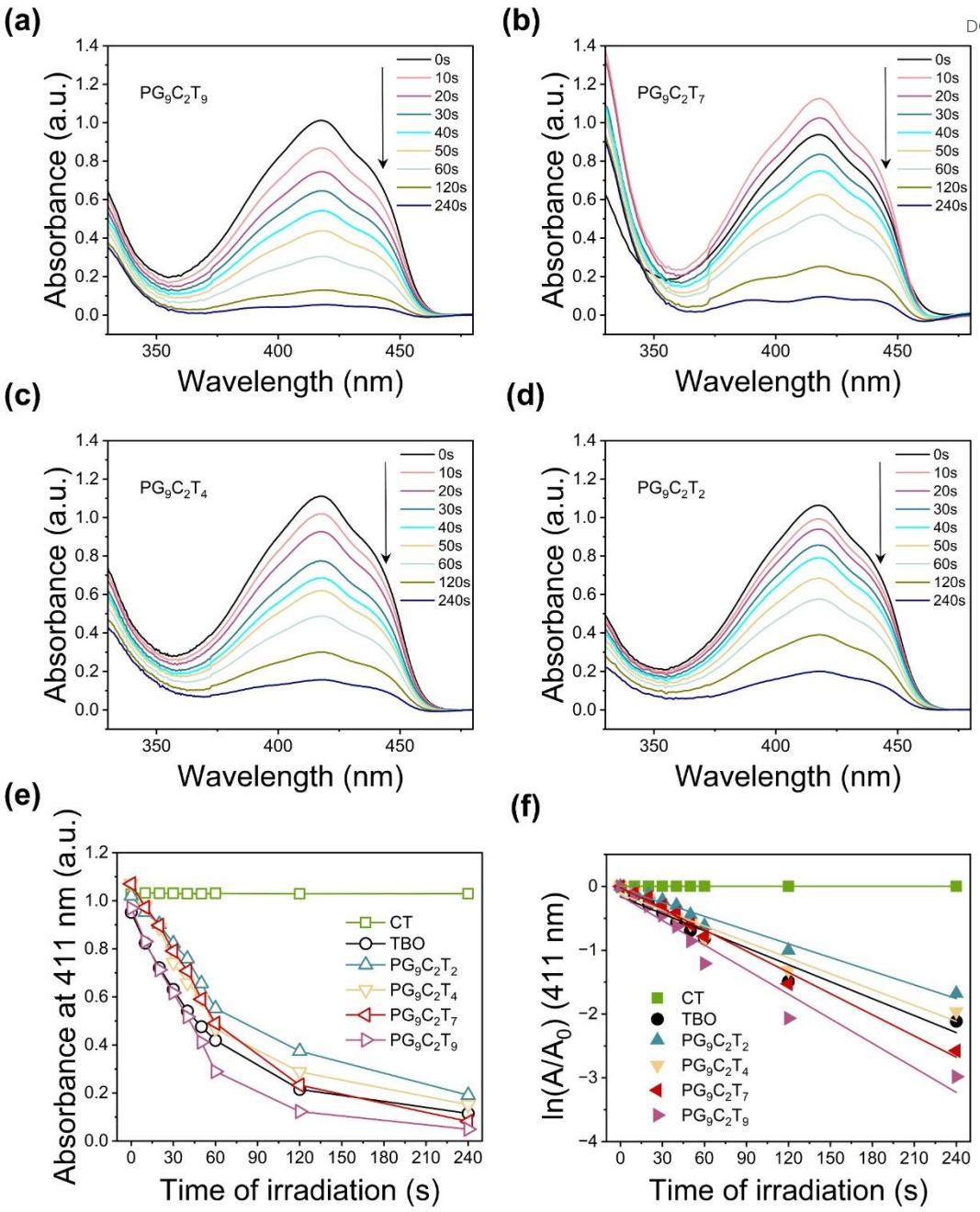

Figure 3. Changes of UV–vis spectra under different irradiation time treated by (a) $PG_9C_2T_9$, (b) $PG_9C_2T_7$, (c) $PG_9C_2T_4$ and (d) $PG_9C_2T_2$. (e) Absorbance decay at 411 nm under different irradiation time. (f) Singlet oxygen productivity kinetics fitted with a pseudo-first order model.

2.3. *In Vitro* Antibacterial Photodynamic Efficiency

To evaluate the *in vitro* photodynamic antibacterial activity of the synthesized polymers, three bacterial strains were selected: *Escherichia coli* (*E. coli*), *Staphylococcus aureus* (*S.*

View Article Online
DOI: 10.1039/D5TB01507C

aureus), and methicillin-resistant *Staphylococcus aureus* (MRSA). The minimum inhibitory concentrations (MICs) of TBO and the polymers were determined according to standard protocols, as shown in Figures 4a–c.

For *E. coli*, in the absence of light irradiation, the MICs of $PG_9C_2T_9$, $PG_9C_2T_7$, and $PG_6C_3T_5$ were 500 $\mu g \cdot mL^{-1}$, which are lower than those of free TBO (2000 $\mu g \cdot mL^{-1}$), because CT appears to play a significant synergistic role in antibacterial activity with TBO. $PG_9C_2T_2$ and $PG_6C_6T_5$ with high CT contents had MICs exceeding 2000 $\mu g \cdot mL^{-1}$, which may be explained by their poor water solubility. Due to the aPDT of TBO, $PG_nC_mT_x$ has lower MICs when illuminated with LEDs at 660 nm as compared to those which are not illuminated. As the degree of ring-opening increased, the MIC of $PG_nC_mT_x$ gradually decreased, suggesting a dose-dependent relationship between antimicrobial efficacy and TBO content. Figure 4a shows that the MIC values of $PG_9C_2T_9$, $PG_9C_2T_7$ and $PG_6C_3T_5$, which exhibit high ring-opening degrees, were determined to be 62.25, 125 and 125 $\mu g \cdot mL^{-1}$ under light irradiation, respectively. The MIC values are considerably lower than those of free TBO (500 $\mu g \cdot mL^{-1}$), suggesting enhanced antibacterial activity, which would be due to a synergistic interaction between CT and TBO. In contrast, $PG_9C_2T_4$ and $PG_9C_2T_2$ (with low ring-opening degrees) showed higher MICs under light exposure than TBO, suggesting that reduced photosensitizer content may diminish antimicrobial activity. Notably, despite exhibiting comparable ring-opening degrees, $PG_6C_6T_5$ and PG_9T_7 (CT-free) demonstrated significantly attenuated antimicrobial efficacy. $PG_6C_6T_5$ is poorly soluble in water due to its high CT content. Conversely, PG_9T_7 lacks CT components, leading to weak interactions with bacteria and reduced aPDT capabilities.

A similar trend was observed for *S. aureus* and MRSA, where higher ring-opening degrees facilitated the synergistic antibacterial properties between TBO and CT (Figure 4b and 4c). As

View Article Online
DOI: 10.1039/D5TB01507C

a result of their low water solubility or weak interaction with bacteria, $PG_9C_2T_2$, $PG_6C_6T_5$ and PG_9T_7 exhibited similar or even higher MICs than TBO under both light and dark conditions. The MICs of the $PG_nC_mT_x$ polymers were lower for Gram-positive bacteria than for Gram-negative bacteria, possibly due to Gram-negative bacteria's outer membrane, which confers enhanced resistance to antibacterial agents. [21, 45]

The plate counting method was employed to quantitatively assess the antibacterial activity of TBO and polymers (Figure 4d and Figure s12-s14). [46] After incubating the test strains with polymers under light irradiation, $PG_9C_2T_9$, $PG_9C_2T_7$ and $PG_6C_3T_5$ showed markedly reduced colony counts compared to TBO. This enhanced activity is likely attributed to strong polymer-bacterial cell interactions, which improve the localized utilization efficiency of $^1O_2$. However, in comparison with TBO, the colony counts of $PG_9C_2T_4$, $PG_9C_2T_2$, $PG_6C_6T_5$ and PG_9T_7 were slightly increased, indicating diminished antibacterial activity. These observations are consistent with MIC results. Based on the quantitative results (Figures 4e–g), high ring-opening $PG_nC_mT_x$ polymers exhibit enhanced bactericidal activity under light irradiation because their lipophilicity facilitates membrane penetration and intracellular $^1O_2$ generation. [31, 47] These results reveal the synergistic antibacterial activity between TBO and CT.

View Article Online
DOI: 10.1039/D5TB01507C

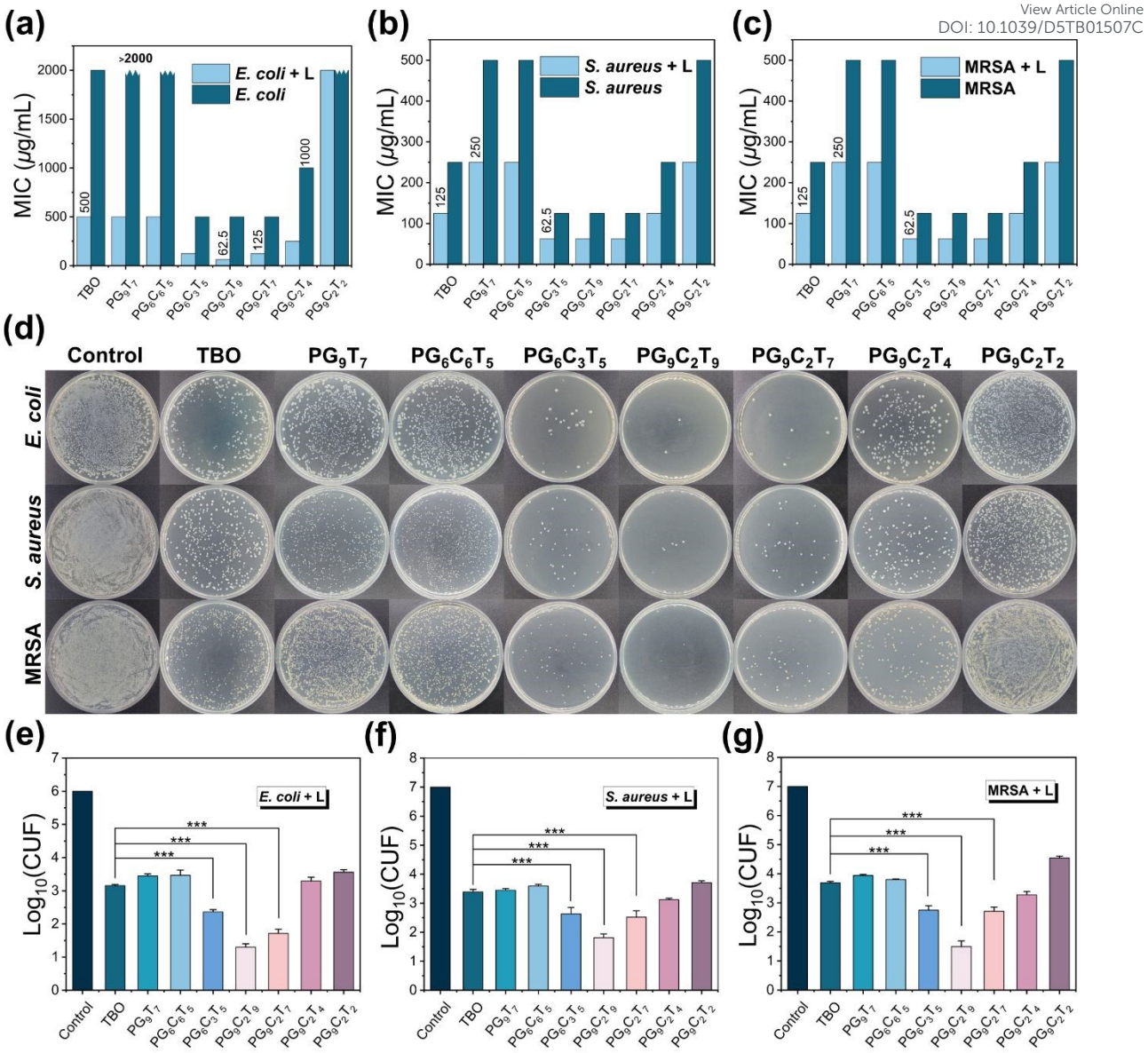

Figure 4. *In vitro* aPDT activity. MICs of TBO and polymers with and without light irradiation against (a) *E. coli*, (b) *S. aureus* and (c) MRSA. (d) Photographs of bacterial colonies formed in LB agar plates after treated with different polymers. The concentrations of polymers are 250 μg mL^{-1} for *E. coli*, 62.5 μg mL^{-1} for *S. aureus* and MRSA. Photobactericidal effect of polymers against (e) *E. coli*, (f) *S. aureus* and (g) MRSA with light irradiation. (*$p < 0.05$, **$p < 0.01$, ***$p < 0.001$). All data are shown as mean ± SD ($n = 3$).

2.4. Accumulations of Polymers in Bacteria

View Article Online
DOI: 10.1039/D5TB01507C

Confocal laser scanning microscopy (CLSM) was employed to visualize the spatial distribution of the photosensitizer in bacteria treated with TBO and $PG_9C_2T_7$ by taking advantage of the intrinsic fluorescence of TBO. According to Fig. 5a, $PG_9C_2T_7$-treated bacteria showed red fluorescence intensity, indicating photosensitizer accumulation. By contrast, bacteria treated with TBO did not exhibit any detectable red fluorescence. [32] The accumulation of polymers within the cells can be more clearly visualized by colocalizing the fluorescent signals with the positions of bacteria in bright-field images.

We evaluated the hemolysis of $PG_nC_mT_x$ polymers using rabbit red blood cells (RBCs), as shown in Figures 5b and 5c. HC_5 refers to the concentration of polymer that causes 5% hemolysis of RBCs. When $PG_nC_mT_x$ was incubated with RBC at 37 °C in the dark for two hours, the hemolysis rate increased as the concentration increased. $PG_nC_mT_x$ can interact with mammals in a nonspecific manner due to its cationic charge. [48] In addition, the hemolysis rate increased after illumination for one hour. The potential cytotoxicity of $^1O_2$ generated by $PG_nC_mT_x$ may account for this effect under light exposure. [49, 50] Furthermore, the hemolysis rate increases with increased ring-opening degree, suggesting that greater TBO content results in greater toxicity.

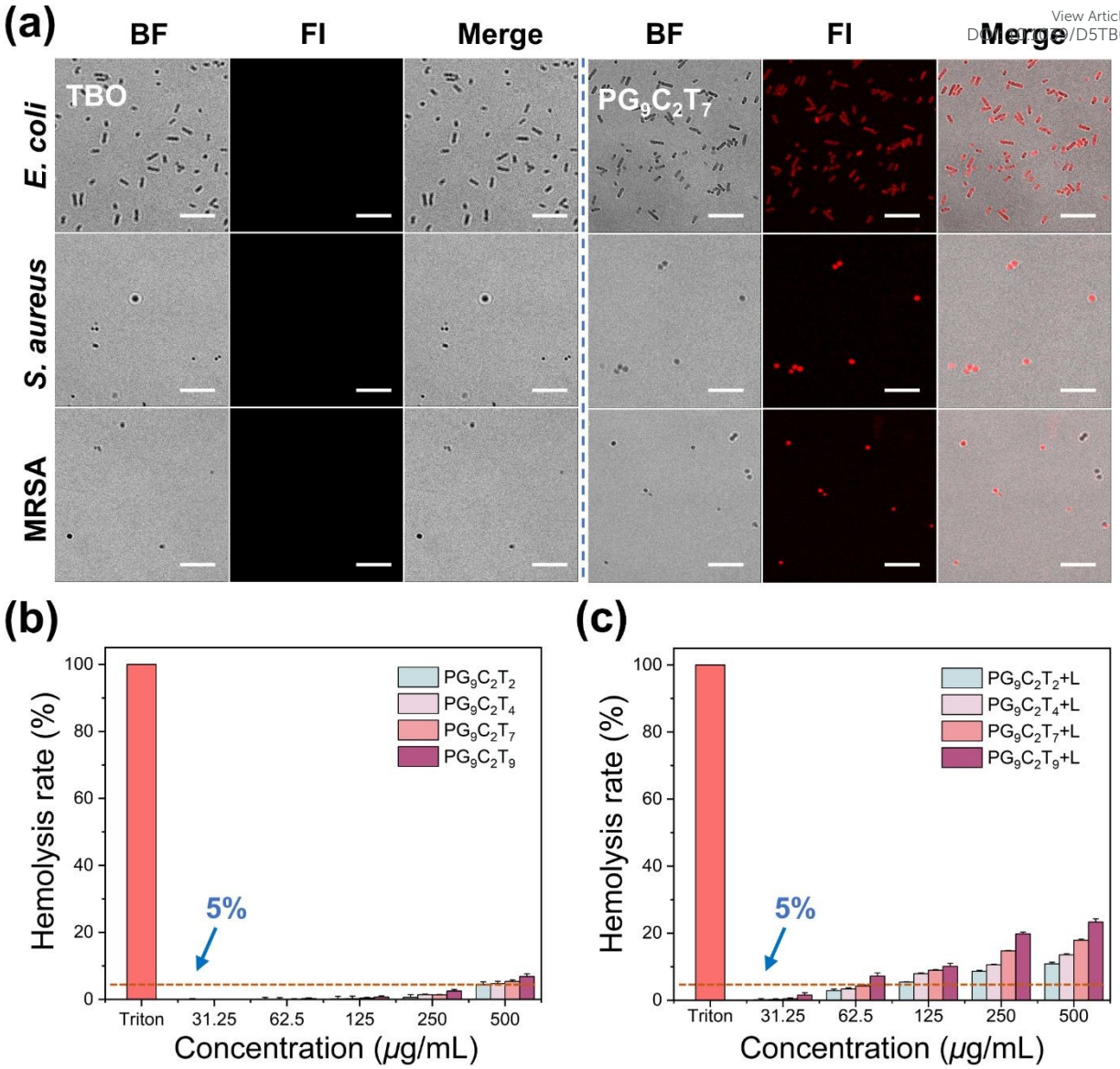

Figure 5. (a) Accumulation of TBO and $PG_9C_2T_7$ in bacteria. Bright field (BF) and fluorescence images (FI) of bacteria incubated with TBO and $PG_9C_2T_7$ observed by CLSM (scale bar: 10 μm). Hemolysis rate of $PG_nC_mT_x$ without (b) and with (c) light irradiation.

2.5. Antibacterial Mechanisms

A LIVE/DEAD BacLight Bacterial Viability Kit was used to assess changes in bacterial membrane permeability before and after polymer treatment using CLSM. To distinguish dead bacteria from viable bacteria, propidium iodide (PI), which selectively permeates compromised bacterial membranes and emits red fluorescence under the excitation at 525 nm, was used to

View Article Online
DOI: 10.1039/D5TB01507C

label dead cells, while SYTO 9 (green fluorescence) stained viable bacteria. As shown in Figure 6a, the test strains in the control group emit obvious green fluorescence with or without 660 nm radiation, indicating a large number of viable bacteria. When these three test strains were incubated with $PG_9C_2T_7$ under light, severe damage to the bacterial membrane occurred, as evidenced by intense PI-derived red fluorescence and significantly reduced SYTO 9-derived green signals. Clearly, this observation indicates membrane damage and altered permeability, accompanied by profound bacterial death. It is noteworthy that limited red fluorescence was observed in dark-incubated samples, attributed to partial bactericidal activity without light activation. Based on these findings, it appears that $PG_9C_2T_7$ exerts photodynamic antibacterial effects primarily by disrupting membranes.

To better understand the interaction mechanism between the polymer and bacteria, scanning electron microscopy (SEM) was employed to analyze morphological changes in bacterial cells before and after treatment with $PG_9C_2T_7$ under light irradiation (Figure 6b). Untreated bacteria (*E. coli*, *S. aureus*, and MRSA) exhibit intact and smooth cellular ultrastructure with well-defined outlines. In contrast, $PG_9C_2T_7$-treated bacteria display extensive membrane deformation and pronounced lysis, indicating that the polymer induces sterilization through structural disruption of bacterial cells. According to the above results, we speculate that the possible antibacterial mechanism is as follows. In water, the amphiphilic $PG_nC_mT_x$ self-assembles into spherical aggregates, and its cationic charge facilitates the binding of bacteria with a negatively charged surface. In addition, the hydrophobicity mediated by citronellol enhances the adhesion of the polymer to the membranes of lipid bilayers, resulting in the enrichment of the polymer by bacteria. Finally, the localized generation of light-induced active ROS drives its efficient synergistic bactericidal activity in the membrane

View Article Online
DOI: 10.1039/D5TB01507C

microenvironment (Figure 1b).

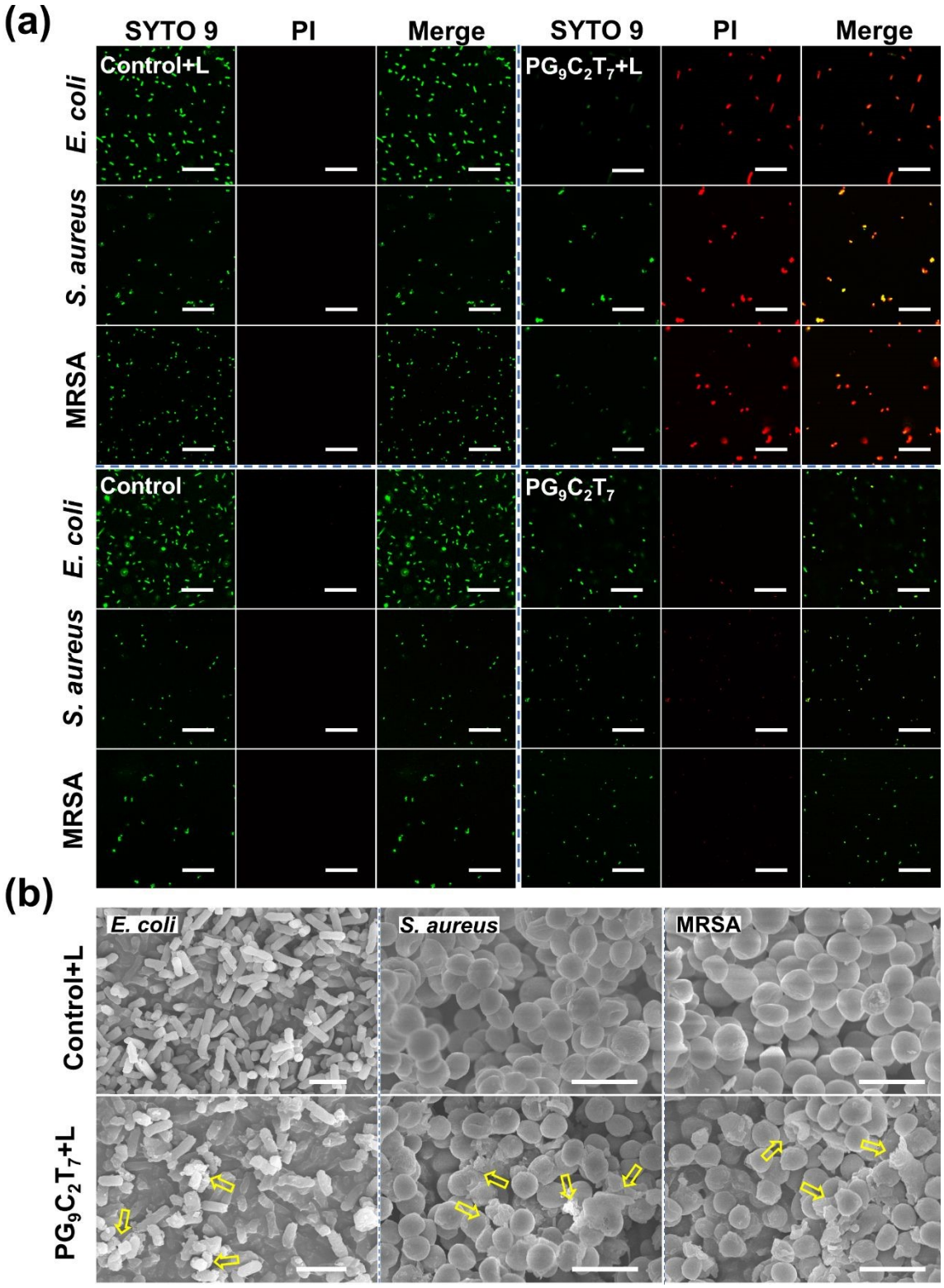

Figure 6. (a). CLSM images of live/dead bacterial treated with $PG_9C_2T_7$ with or without light irradiation (scale bars: 25 μm). (b). SEM images of $PG_9C_2T_7$ treated bacteria with light irradiation (scale bars: 3 μm).

View Article Online
DOI: 10.1039/D5TB01507C

2.6. Preparations and Characterizations of light-activated antimicrobial PDMS (LAPDMS)

The $PG_nC_mT_x$ was further explored for incorporation into PDMS to produce LAPDMS. PDMS is one of the most extensively utilized polymeric biomaterials in medical devices. [51] PDMS were prepared from the SYLGARDTM 184 Silicone elastomer base and its curing agent by casting into appropriate molds for the experiments and curing at 25 °C for 48 h (Figure 7a). LAPDMS were then fabricated using a 'swell-encapsulation-shrink' method. [44, 52] LAPDMS stability and $PG_nC_mT_x$ leaching were assessed using UV-visible absorption analysis (Figure 7b). There was a negligible change in absorbance at 635 nm (attributed to $PG_9C_2T_7$) after 4 hours of immersion, indicating that $PG_9C_2T_7$ was minimally released from PDMS. With minimal leaching, adverse effects on surrounding tissues can be reduced by limiting the amount of $PG_9C_2T_7$ that comes into direct contact with and penetrates them.

We evaluated the antibacterial activity of LAPDMS using the viable cell count method. [53] LAPDMS was cocultured with bacterial suspensions under illumination for a variety of durations, and pristine PDMS was used as a control. Figure 7c shows that LAPDMS-treated groups under illumination exhibited significantly fewer colonies than other groups (Figure S15). After only one hour of illumination, there was a significant difference in colony counts, and the colony count was reduced by 1–3 logs after two to eight hours of illumination, and complete sterilization was achieved after 12 hours of continuous illumination. LAPDMS exhibits bactericidal properties due to the unique photoactivation mechanism of the adsorbed $PG_nC_mT_x$ polymers, which destroy the structure of microbial cells. In other groups, a slight decrease in colony numbers may be attributed to natural microbial decay.

LAPDMS was then tested for antibacterial adhesion properties according to a previously

View Article Online
DOI: 10.1039/D5TB01507C

reported assay. [53] LAPDMS and pristine PDMS surfaces were soaked in bacterial suspension and cultured for 4 hours at 37 °C. Bacteria loosely attached to the surface were washed off with phosphate buffer saline. By sonication and vortexing, the attached bacteria were then removed from the PDMS surface and spread on LB agar plates. As illustrated in Figure 7d, the number of *S. aureus* colonies recovered from LAPDMS was significantly less than that from pristine PDMS, demonstrating that LAPDMS is effective at preventing bacterial adhesion. As shown in Figure 7e, both pristine PDMS and LAPDMS exhibited minimal hemolytic activity, with hemolysis rates < 5%. Following light exposure for one hour, LAPDMS showed a slight increase in hemolysis, reaching 8.6%.

View Article Online
DOI: 10.1039/D5TB01507C

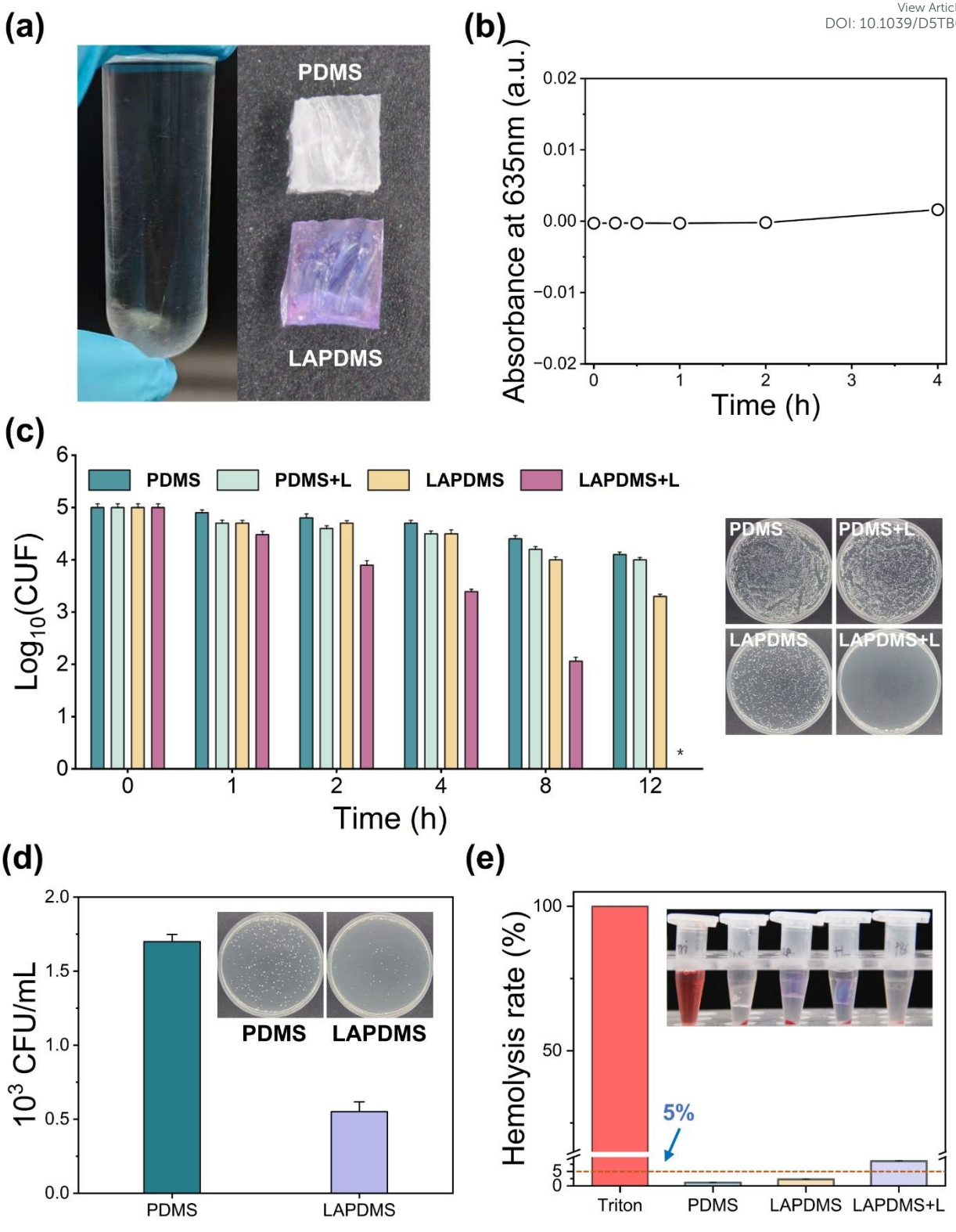

Figure 7. (a) Photographic images of pristine PDMS and LAPDMS. (b) Absorption intensity at 635 nm corresponding to $PG_9C_2T_7$ after LAPDMS has been immersed in water for different periods of time. (c) In vitro evaluation of the bactericidal activity of pristine PDMS and LAPDMS against *S. aureus* with or without light irradiation; the photographs of bacterial

View Article Online
DOI: 10.1039/D5TB01507C

colonies formed on LB agar plates after treatment with pristine PDMS and LAPDMS for 12 h (right). (d) The bacterial density detached from pristine PDMS and LAPDMS; the inset shows the LB agar plates. (e) Hemolysis analysis for pristine PDMS and LAPDMS with or without light irradiation.

3. Conclusion

In summary, we have designed and synthesized a novel CT-enhanced photobaceticidal polymer $PG_nC_mT_x$ and successfully constructed a light-activated antimicrobial PDMS. The polymers combined with TBO and CT demonstrated significantly enhanced antibacterial activity compared to TBO. It should be noted that $PG_9C_2T_9$, $PG_9C_2T_7$, and $PG_6C_3T_5$ exhibited superior antibacterial activity, while PG_9T_7 without CT showed reduced efficacy compared with free TBO, highlighting the synergistic interaction between TBO and CT. CT enables the polymer to self-assemble and enhances the interaction between the polymer and bacteria, while also promoting the accumulation of TBO within cells by improving membrane permeability. ROS generated in specific subcellular regions maximizes photodynamic therapy's therapeutic potential. Additionally, the prepared LAPDMS exhibit good biocompatibility while achieving complete sterilization in 12 h. The findings offer valuable insights for designing highly effective, low-toxicity photobaceticidal polymers and lay the groundwork for antibacterial photodynamic therapy's potential applications.

4. Experimental Section

Materials and apparatus: β-Citronellol (CT, 95%) and Methacryloyl chloride (95%) were purchased from Aladdin. Methyl 2-bromo-2-methylpropionate (MeBrMP, 99%), Glycidyl

View Article Online
DOI: 10.1039/D5TB01507C

methacrylate (GMA, 98%), 2,2′-bipyridine (BPY, 98%) and anhydrous triethylamine (TEA), dichloromethane (CH_2Cl_2), tetrahydrofuran (THF) were purchased from Energy Chemical. Toluidine blue O (TBO) was purchased from Macklin. All chemicals were used as received. CuBr was washed with acetic acid and anhydrous ethanol successively and then dried in vacuum before using. SYLGARDTM 184 Silicone elastomer base and its curing agent were perchased from Dow Corning. *E. coli* (ATCC 25922), *S. aureus* (ATCC 25923) and MRSA (ATCC 43300) were purchased from Guangdong Huankai Microbial Sci. & Tech. Co., Ltd. and incubated before use. ^{1}H NMR spectra were measured on a Bruker Avance III HD 400 instrument using TMS as an internal standard. The polymer dispersity index (PDI) of the polymers was measured by GPC with THF as the mobile phase using Waters Advanced Polymer Chromatography (ACQYITY APC) with an ACQUITY APC XT column. Polystyrene with a narrow distribution is used as the calibration standard.

Synthesis of CMA: CT (1.8 mL, 10 mmol), TEA (1.7 mL, 12 mmol) were charged into a three-necked round-bottom flask equipped with a nitrogen inlet. Methacryloyl chloride (1.2 mL, 12 mmol) was introduced dropwise via a pressure-equalizing dropping funnel while maintaining the reaction mixture at 0–5°C in an ice-water bath. Following the addition, the reaction was allowed to proceed under continuous stirring at 30°C for 8 h. The crude product was purified by flash chromatography on a silica gel column and subsequently dried under vacuum at 25°C for 24 h to yield the target monomer.

Synthesis of PG_nC_m : Taking PG_9C_2 as an example, MeBrMP (0.5 mL, 3.9 mmol), GMA (5 mL, 38 mmol), CMA (1.7 g, 7.5 mmol), and BPY (0.61 g, 3.9 mmol) were added into the Schlenk flask and dissolved in THF (15 mL). The reaction mixture was subjected to three cycles of freeze-pump-thaw degassing under a nitrogen atmosphere. Subsequently, CuBr (0.56 g, 3.9

mmol) was introduced, and the system underwent two additional degassing cycles. The sealed flask was then maintained at 50°C with continuous stirring for 12 h. The polymerization reaction was quenched by rapid cooling in liquid nitrogen, followed by dilution with THF. Residual copper complexes were removed *via* filtration through an Al_2O_3 column. The organic phase was concentrated under reduced pressure and precipitated twice in cold methanol. The resultant polymer was vacuum-dried at 35°C for 24 h. PG_n without CMA was synthesized following an analogous protocol.

Synthesis of $PG_nC_mT_x$: Taking $PG_9C_2T_9$ as an example, PG_9C_2 (0.1 g, 0.05 mmol), TBO (0.45 g, 1.5 mmol) and hydrochloric acid (10% mmol) were added into a 25 mL round bottom flask and dissolved in DMSO (5 mL). The reaction mixture was maintained under dark conditions with continuous stirring at 25°C for 8 h under a nitrogen atmosphere. The crude product was purified by dialysis using a dialysis bag (MWCO 500) in deionized water for 48 h. Following solvent evaporation and removal of unreacted TBO, the residue was subjected to lyophilization under vacuum for 24 h to yield the ring-opened product $PG_9C_2T_7$.

Quantum yields and kinetics of $^1O_2$: TBO and polymers were introduced into a 0.05 mM DPBF solution under continuous stirring until complete dissolution. The homogeneous mixture was irradiated with a 660 nm LED light source (power density: 20 mW cm^{-2}), and the temporal decay of DPBF absorbance at 411 nm was monitored at predetermined time intervals to quantify $^1O_2$ generation kinetics.

Minimum inhibitory concentrations (MIC): *E. coli*, *S. aureus* and MRSA were inoculated into a lysogeny broth (LB) medium and incubated overnight at 200 rpm at 37 °C. The cultured bacterial suspension (20 μL) was transferred to a fresh LB medium (2 mL) and incubated to the mid-exponential developmental stage. The bacterial suspensions were diluted to OD_{600} = 0.1 in

View Article Online
DOI: 10.1039/D5TB01507C

LB medium to obtain the working suspension. 2-Fold serial dilution of TBO and polymers was performed in a 96-well plate with LB medium, and the bacterial working suspension (20 μL) was added to the well and then the plate was gently shaken for 10 s. The final concentrations of TBO and polymers were 2000, 1000, 500, 250, 125, 62.5, 31.25, and 15.625 μg mL^{-1}, and the total volume of each well was 200 μL. The plate was exposed to a 660 nm LED light source for 1 h and then incubated at 37 °C for 18 h. The experiments in different concentrations were repeated three times in parallel with setting a positive control (180 μL of LB medium and 20 μL of bacterial suspension) and a negative control (200 μL of LB medium). The MIC value was determined to be the lowest concentration with no visible bacterial growth at 18 h after incubation at 37 °C.

Plate counting assays: The bacterial concentrations of *E. coli*, *S. aureus* and MRSA were approximately 10^6 CFU mL^{-1} ,10^7 CFU mL^{-1} and 10^7 CFU mL^{-1}, respectively. 100 μL of bacterial culture medium and 100 μL TBO, polymers solutions were incubated in the dark at 37 ℃ with 200 rpm for 30 min. The final concentrations of TBO and polymers were 500, 250, 125, 62.5, 31.25, and 15.625 μg mL^{-1}. Subsequently, 200 μL of the mixture was spread onto LB broth agar medium. The agar plates were then exposed to a 660 nm LED light source for 1 h and incubated at 37 ℃ for 24 h to observe bacterial growth.

Polymer accumulation assays: The bacterial suspensions were incubated with TBO and $PG_9C_2T_7$ for 30 min in the dark. Afterward, the bacterial suspensions were subjected to centrifugation at 5000 rpm for 5 min to gather the bacterial cells. The cells were washed with PBS multiple times. Fluorescence images of the bacterial cells after washing were captured using a CLSM.

Hemolytic activity assays: To determine the toxicity to rabbit RBCs of polymers, $PG_9C_2T_x$ were

View Article Online
DOI: 10.1039/D5TB01507C

incubated with RBCs, and hemolysis was obtained by a hemoglobin release assay. The fresh RBCs were washed with PBS three times and centrifuged for 5 min at 3000 rpm to get erythrocytes. RBCs (0.5 g) were resuspended in PBS (9.5 g) to prepare a 5% RBC suspension. PBS (0.5 mL) or 0.2% Triton X-100 (0.5 mL) was added to a 5% RBC (0.5 mL) suspension as a negative and positive control, respectively. $PG_9C_2T_x$ (0.5 mL) solution in PBS with various concentrations was added to 0.5 mL of 5% RBC suspension (c = 31.25−1000 μg mL^{-1}), and the mixture was exposed to a 660 nm LED light source for 1 h and incubated at 37 °C for 1 h. The sample was centrifuged at 3000 rpm for 5 min, and then photographs were taken after that. The supernatant (100 μL) was transferred to a 96-well plate, and the absorbance at 540 nm was detected by a microplate reader (Cytation5), and the hemolysis rate was calculated by the following formula: Hemolysis ratio (%) = $\left[(OD_{samp} - OD_{neg}) / (OD_{pos} - OD_{neg})\right] \times 100$

Live/Dead bacterial staining: The integrity of the bacterial membrane can be detected by confocal laser scanning microscopy (CLSM, TCS SPE) with LIVE/DEAD BacLight Bacterial Viability Kits. The bacterial working suspension was mixed with $PG_9C_2T_7$ for 30 min under dark condition with the final concentration of 125 μg mL^{-1} for *E. coli*, 62.5 μg mL^{-1} for *S. aureus* and MRSA, and then the mixture was exposed to a 660 nm LED light source for 1 h. The suspension (1 mL) was collected and centrifuged for 5 min at 5000 rpm and then the supernatant was removed and washed with PBS twice. The bacteria were resuspended in PBS (1 mL) and SYTO9 (1.5 μL) and PI (1.5 μL) were added. The suspension was incubated for 15 min in the dark, and 10 μL was dripped onto the microscope slide. The fluorescence was observed by CLSM with dual channels. The excitation wavelength for SYTO 9 and PI is 488 and 535 nm, respectively. The emission for SYTO 9 and PI is 500−540 and 583−688 nm, respectively.

View Article Online
DOI: 10.1039/D5TB01507C

Morphological changes of bacteria: A bacterial suspension (5 mL, 10^8 CFU mL^{-1}) mixed with $PG_9C_2T_7$ was incubated for 30 min in the dark, followed by light irradiation for 1 h. Then, 1 mL of the mixture was collected and centrifuged at 5000 rpm for 5 min, followed by collecting the precipitation and washing with PBS. The samples were fixed in 2.5% glutaraldehyde for 12 h at 4 °C. Afterward, the samples were dehydrated with a series of graded ethanol solutions (30, 50, 70, 85, 95, and 100%) for 10 min. The dehydrated samples were dried and used for SEM (FE-SEM, Hitachi) characterization.

Preparations of PDMS and LAPDMS: The viscous liquid PDMS precursor and its curing agent were mixed at a 10:1 volume ratio in a beaker. The mixture was vigorously stirred using a glass rod to ensure homogeneity, followed by 10 min of ultrasonication to eliminate air bubbles. The mixture was then carefully transferred into a 50 mL centrifuge tube and cured at 25°C for 48 h. The LAPDMS was fabricated using a 'swell-encapsulation-shrink' method. Briefly, a 5 mg mL^{-1} solution of polymer $PG_9C_2T_7$ was prepared in a mixed solution of DMSO and $CHCl_3$. The PDMS substrates were immersed in this polymer solution for 4 h to achieve swelling. After immersion, the samples were washed gently with PBS, followed by drying in a 40°C oven to remove the residual solvents.

Leaching assay: The fabricated LAPDMS was placed in deionized water, and the UV-vis absorption spectra of the solution were obtained every 30 min for a total of 4 h. The absorption intensity of polymer $PG_9C_2T_7$ at 635 nm was recorded.

Antibacterial kinetics of LAPDMS: *S. aureus* was selected as the model strain and the bacterial concentration was approximately 10^6 CFU mL^{-1}. Pristine PDMS and LAPDMS were incubated with the prepared bacterial suspension at 37°C with illumination for different times. At set timepoints, 100 μL of the suspension was plated onto LB agar plates for colony counting.

View Article Online
DOI: 10.1039/D5TB01507C

Anti-adhesion assays of LAPDMS: The *S. aureus* suspension was standardized to a concentration of 10^7 CFU mL^{-1}. Pristine PDMS and LAPDMS were placed in a 24-well plate, each incubated with 1 mL of the bacterial suspension under 37°C with illumination for 4 h. Subsequently, the samples were gently washed with PBS to remove non-specifically adhered bacteria and then were transferred to centrifuge tubes containing 3 mL PBS, followed by 6 min of ultrasonic treatment and 15 s of vortex oscillation. The bacterial suspension was diluted in PBS and plated onto LB agar plates for colony counting.

Statistical analysis

Statistical analysis was conducted using Origin2025SR1 software and was performed to assess significant differences between groups using two-way ANOVA with a multiple-comparison test. The results were expressed as mean ± SD. In the figures, asterisks represent the following p values: *$p < 0.05$, **$p < 0.01$, ***$p < 0.001$, and ****$p < 0.0001$, ns, no significant.

Author contributions

Jiahao Ling: writing – original draft, validation, investigation, visualization, data curation, conceptualization. Chuming Pang: writing – editing, methodology, investigation, visualization, data curation. Tingxin Tan: writing – editing, methodology, data curation. Liangzhi Hong: writing – review & editing, methodology, conceptualization, supervision.

Data availability

The data supporting this article have been included as part of the ESI.

Conflicts of interest

View Article Online
DOI: 10.1039/D5TB01507C

The authors declare no conflict of interest.

Acknowledgements

This work was financially supported by the National Natural Science Foundation of China (21774035), the Key Laboratory of Polymeric Composite and Functional Materials of Ministry of Education (PCFM-2022A05), Guangdong Provincial Key Laboratory of Luminescence from Molecular Aggregates, China (2023B1212060003).

References

1. N. Kipshidze, N. Yeo and N. Kipshidze, *Nat. Photon.*, 2020, **14**, 651-652.
2. S. V. Lynch and O. Pedersen, *N. Engl. J. Med.*, 2016, **375**, 2369-2379.
3. D. Rybak, J. Du, P. Nakielski, C. Rinoldi, A. Kosik-Koziol, A. Zakrzewska, H. Wu, J. Li, X. Li, Y. Yu, B. Ding and F. Pierini, *Adv. Healthcare Mater.*, 2025, **14**, 2404274.
4. N. Xu, Y. Yuan, L. Ding, J. Li, J. Jia, Z. Li, D. He and Y. Yu, *Burns Trauma*, 2022, **10**, tkac019.
5. N. Xu, Y. Gao, Z. Li, Y. Chen, M. Liu, J. Jia, R. Zeng, G. Luo, J. Li and Y. Yu, *Chem. Eng. J.*, 2023, **466**, 143173.
6. R. Singh, A. P. Singh, S. Kumar, B. S. Giri and K.-H. Kim, *J. Clean. Prod.*, 2019, **234**, 1484-1505.
7. R. Aggarwal, M. Pooja, P. Sameeksha, B. Aayushi, V. S. Kumar, Y. Puja, K. A. S., K. A. Ullah, D. Meenakshi and A. K. and Johri, *Crit. Rev. Microbiol.*, 2024, **50**, 896-921.
8. J. Davies and D. Davies, *Microbiol. Mol. Biol. Rev.*, 2010, **74**, 417-433.
9. J. M. A. Blair, M. A. Webber, A. J. Baylay, D. O. Ogbolu and L. J. V. Piddock, *Nat. Rev. Microbiol.*, 2014, **13**, 42-51.
10. W. P. J. Smith, B. R. Wucher, C. D. Nadell and K. R. Foster, *Nat. Rev. Microbiol.*, 2023,

View Article Online
DOI: 10.1039/D5TB01507C

21, 519-534.

11. X. J. Hu, H. Zhang, Y. T. Wang, B. C. Shiu, J. H. Lin, S. J. Zhang, C. W. Lou and T. T. Li, *Chem. Eng. J.*, 2022, **450**, 138129.
12. C. Elian, R. Méallet and D. L. Versace, *Adv. Funct. Mater.*, 2024, **34**, 2407228.
13. V. N. Nguyen, Z. Zhao, B. Z. Tang and J. Yoon, *Chem. Soc. Rev.*, 2022, **51**, 3324-3340.
14. P. R. Judzewitsch, N. Corrigan, E. H. H. Wong and C. Boyer, *Angew. Chem. Int. Ed.*, 2021, **60**, 24248-24256.
15. Z. Shao, H. Sun and E. H. H. Wong, *Polym. Chem.*, 2025, **16**, 1373-1382.
16. B. Wang, M. Wang, A. Mikhailovsky, S. Wang and G. C. Bazan, *Angew. Chem. Int. Ed.*, 2017, **56**, 5031-5034.
17. M. Zheng, H. Lin, W. Zhang, S. Tang, D. Liu and J. Cai, *ACS Infect. Dis.*, 2021, **7**, 2917-2929.
18. G. B. Kharkwal, S. K. Sharma, Y.-Y. Huang, T. Dai and M. R. Hamblin, *Lasers Surg. Med.*, 2011, **43**, 755-767.
19. L. Sobotta, P. Skupin-Mrugalska, J. Piskorz and J. Mielcarek, *Eur. J. Med. Chem.*, 2019, **175**, 72-106.
20. S. Kwiatkowski, B. Knap, D. Przystupski, J. Saczko, E. Kędzierska, K. Knap-Czop, J. Kotlińska, O. Michel, K. Kotowski and J. Kulbacka, *Biomed. Pharmacother.*, 2018, **106**, 1098-1107.
21. Q. Jia, Q. Song, P. Li and W. Huang, *Adv. Healthcare Mater.*, 2019, **8**, 1900608.
22. S. Liu, H. Yuan, H. Bai, P. Zhang, F. Lv, L. Liu, Z. Dai, J. Bao and S. Wang, *J. Am. Chem. Soc.*, 2018, **140**, 2284-2291.
23. Q. Lei, D. He, L. Ding, F. Kong, P. He, J. Huang, J. Guo, C. J. Brinker, G. Luo, W. Zhu and Y. Yu, *Adv. Funct. Mater.*, 2022, **32**, 2113269.
24. J. Moan and K. Berg, *Photochem. Photobiol.*, 1991, **53**, 549-553.
25. B. Ran, Z. Wang, W. Cai, L. Ran, W. Xia, W. Liu and X. Peng, *J. Am. Chem. Soc.*,

2021, **143**, 17891-17909.

View Article Online
DOI: 10.1039/D5TB01507C

26. J. A. Williams, G. J. Pearson, M. J. Colles and M. Wilson, *Caries Res.*, 2004, **38**, 530-536.

27. I. C. J. Zanin, M. M. Lobo, L. K. A. Rodrigues, L. A. F. Pimenta, J. F. Höfling and R. B. Gonçalves, *Eur. J. Oral Sci.*, 2006, **114**, 64-69.

28. Y. He, J. Pang, Z. Yang, M. Zheng, Y. Yu, Z. Liu, B. Zhao, G. Hu and R. Yin, *Photodiagnosis Photodyn Ther.*, 2022, **39**, 102902.

29. L. Misba, H. Abdulrahman and A. U. Khan, *Photodiagnosis Photodyn Ther.*, 2019, **26**, 383-388.

30. Y. Zheng, E. Yu, Q. Weng, L. Zhou and Q. Li, *Lasers Med. Sci.*, 2019, **34**, 1535-1545.

31. J. Robinson-Duggon, N. Pizarro, G. Gunther, D. Zúñiga-Núñez, A. M. Edwards, A. Greer and D. Fuentealba, *Photochem. Photobiol.*, 2021, **97**, 71-79.

32. X. Gu, H. Yuan, C. Li, L. Xu, S. Li and D. Yu, *Colloids Surf. B Biointerfaces*, 2024, **233**, 113657.

33. B. Rout, C.-H. Liu and W.-C. Wu, *Sci. Rep.*, 2017, **7**, 7892.

34. P. L. Santos, J. P. S. C. F. Matos, L. Picot, J. R. G. S. Almeida, J. S. S. Quintans and L. J. Quintans-Júnior, *Food Chem. Toxicol.*, 2019, **123**, 459-469.

35. T. Wei, C. Regeard, N. Barroca-Aubry, P. Roger and C. Aymes-Chodur, *Colloids Surf. B Biointerfaces*, 2025, **253**, 114723.

36. Q.-B. D. Nguyen, M.-A. N. Vu and A. A. Hebert, *J. Am. Acad. Dermatol.*, 2023, **88**, 123-130.

37. N. Agrawal, G. L. Maddikeri and A. B. Pandit, *Ultrason. Sonochem.*, 2017, **36**, 367-374.

38. S. G. Griffin, S. G. Wyllie, J. L. Markham and D. N. Leach, *Flavour Fragr. J.*, 1999, **14**, 322-332.

39. Mulyaningsih, F. Sporer, J. Reichling and M. Wink, *Pharm. Biol.*, 2011, **49**, 893-899.

40. L. Lian, C. Pang, H. Wei and L. Hong, *Macromol. Biosci.*, 2023, **23**, 2300169.

41. J. Yook, D. Jeong and J.-C. Lee, *Macromolecules*, 2023, **56**, 3406-3420.

42. Y. Wu, D. Hong, S. Qiu, Y. Fang and Y. Zhu, *Polym. Test.*, 2024, **140**, 108582.

43. T. Entradas, S. Waldron and M. Volk, *J. Photochem. Photobiol. B: Biol.*, 2020, **204**, 111787.

44. S. Ghaffari, N. Amiri, D. F. Felix, S. Abbasidezfouli, F. Franco, S. L. Beaupré, N. R. Branda and D. Lange, *Colloids Surf. B Biointerfaces*, 2024, **233**, 113637.

45. C. Pang, B. Li, Z. Tu, J. Ling, Y. Tan, S. Chen and L. Hong, *ACS Appl. Mater. Interfaces*, 2024, **16**, 38429-38441.

46. L. Yang, C. Zhan, X. Huang, L. Hong, L. Fang, W. Wang and J. Su, *Adv. Healthcare Mater.*, 2020, **9**, 2000186.

47. M. Wainwright, C. O'Kane and S. Rawthore, *J. Photochem. Photobiol. B: Biol.*, 2016, **160**, 68-71.

48. M. Jurak, A. E. Wiącek, A. Ładniak, K. Przykaza and K. Szafran, *Adv. Colloid Interface Sci.*, 2021, **294**, 102451.

49. J.-Q. Chu, D.-X. Wang, L.-M. Zhang, M. Cheng, R.-Z. Gao, C.-G. Gu, P.-F. Lang, P.-Q. Liu, L.-N. Zhu and D.-M. Kong, *ACS Appl. Mater. Interfaces*, 2020, **12**, 7575-7585.

50. Y. Zhu, C. Xu, N. Zhang, X. Ding, B. Yu and F.-J. Xu, *Adv. Funct. Mater.*, 2018, **28**, 1706709.

51. J. J. Dong, A. Muszanska, F. Xiang, R. Falkenberg, B. van de Belt-Gritter and T. Loontjens, *Langmuir*, 2019, **35**, 14108-14116.

52. S. Noimark, E. Allan and I. P. Parkin, *Chem. Sci.*, 2014, **5**, 2216-2223.

53. B. Li, C. Pang, S. Chen and L. Hong, *Macromol. Rapid Commun.*, 2024, **45**, 2400170.

View Article Online
DOI: 10.1039/D5TB01507C

Data availability

The authors confirm that the data supporting the findings of this study are available within the article and Supplementary Material. Raw data and support the findings of this study are available from the corresponding author, upon reasonable request.